

Overcoming the Rate-Directionality Trade-off: A Room-Temperature Ultrabright Quantum Light Source

Hamza Abudayyeh, Annika Mildner, Dror Liran, Boaz Lubotzky, Lars Lüder, Monika Fleischer, and Ronen Rapaport*



Cite This: <https://doi.org/10.1021/acsnano.1c08591>



Read Online

ACCESS |



Metrics & More



Article Recommendations



Supporting Information

ABSTRACT: Deterministic GHz-rate single photon sources at room temperature would be essential components for various quantum applications. However, both the slow intrinsic decay rate and the omnidirectional emission of typical quantum emitters are two obstacles toward achieving such a goal which are hard to overcome simultaneously. Here, we solve this challenge by a hybrid approach using a complex monolithic photonic resonator constructed of a gold nanocone responsible for the rate enhancement, enclosed by a circular Bragg antenna for emission directionality. A repeatable process accurately binds quantum dots to the tip of the antenna-embedded nanocone. As a result, we achieve simultaneous 20-fold emission rate enhancement and record-high directionality leading to an increase in the observed brightness by a factor as large as 800 (130) into an NA = 0.22(0.5). We project that these miniaturized on-chip devices can reach photon rates approaching 1.4×10^8 photons/s and pure single photon rates of $>10^7$ photons/second after temporal purification processes, thus enabling ultrafast light–matter interfaces for quantum technologies at ambient conditions.

KEYWORDS: single-photon source, quantum dots, colloidal nanocrystals, Purcell factor, plasmonic resonator, nanoantenna, directional emission



Quantum light sources have witnessed rapid developments in the last few decades culminating in state of the art results primarily using quantum dot sources¹ and multiplexed parametric sources.² As a result, attempts have been made to use single photon sources in realistic quantum applications. For example, a quantum dot source was recently used to feed a 60 mode Boson sampler³ resulting in a Hilbert space on the order of 10^{14} . Semiconductor quantum dot sources were also utilized for quantum computation purposes by demonstrating a high fidelity controlled-NOT gate^{4,5} and more recently generating a photonic cluster state.^{6,7} For a quantum key distribution (QKD), for example, operation over a fiber-link of 120 km was demonstrated using a single quantum dot source.⁸ More recently, entangled photon pairs, emanating from a space-borne parametric source, were distributed to two distant ground locations separated by 1200 km.⁹ These significant efforts point to the importance of developing bright single photon sources approaching GHz photon rates in order to enable realistic deployment of such technologies.¹⁰ Solid-state emitters, *e.g.*, self-assembled quantum dots (SAQDs),¹¹ defects in crystals,¹² and colloidal quantum dots (CQDs),^{13,14} offer distinct advantages including superior single photon properties and the convenience and

scalability of a solid-state matrix. However, solid-state emitters typically have isotropic emission and a radiative lifetime on the order of several to hundreds of nanoseconds in the absence of any photonic structure. This eventually leads to a severe restriction in terms of the useful photonic rate that can be collected into the desired mode.

Engineering both the decay rate and the emission pattern, however, is no trivial task. This is clarified in Figure 1A, which shows the typical trade-offs associated with such an endeavor: in the presence of an optical resonator the rate of an emitter is modified by the Purcell factor which is proportional to $\frac{Q}{V}$ (Q is the quality factor and V is the mode volume), whereas the angular emission pattern is Fourier limited by the mode volume. Therefore, in a *single* resonator, both a high Q factor

Received: September 29, 2021

Accepted: October 14, 2021

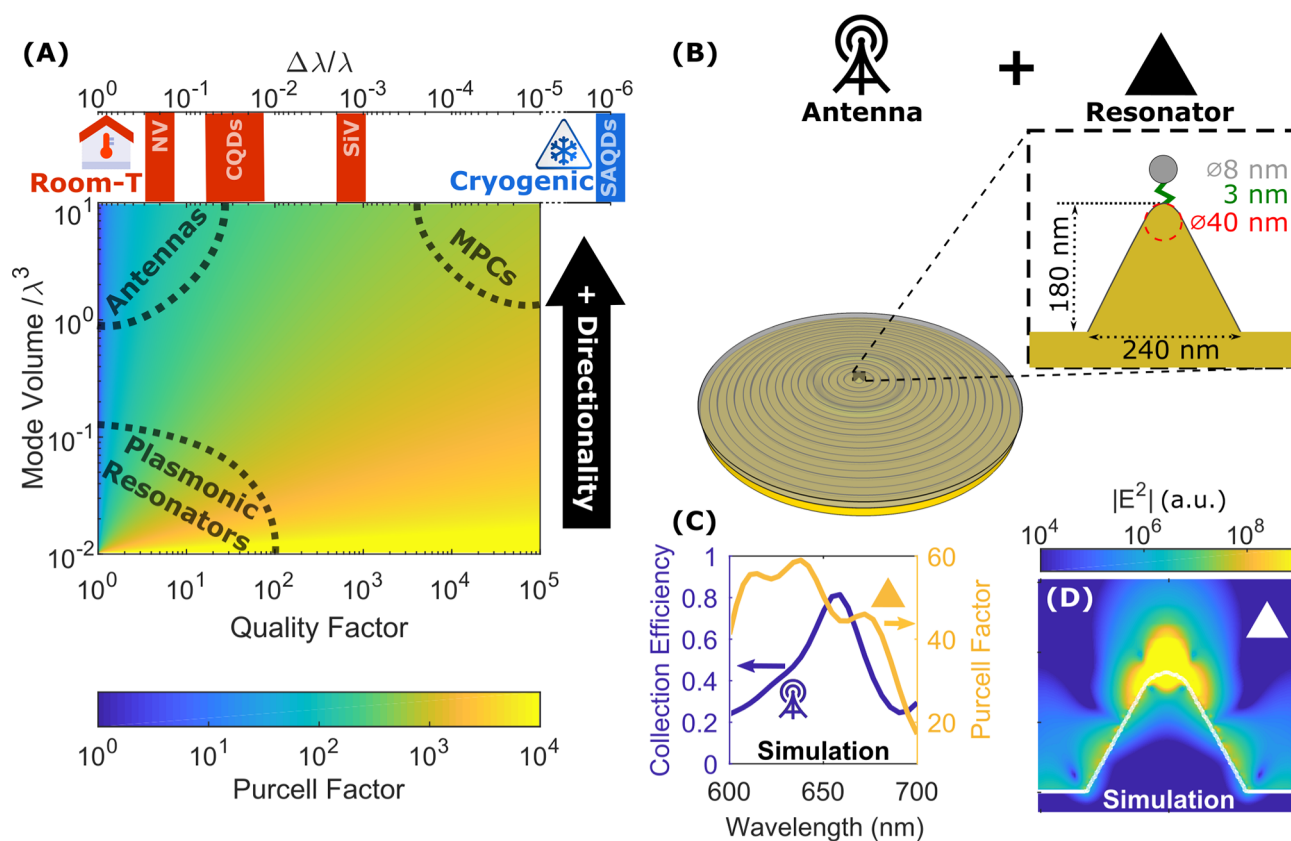


Figure 1. Overview of the trade-off between rate enhancement and directionality for room-temperature sources. (A) The color plot displays the Purcell factor as a function of the quality factor and mode volume in the weak coupling regime. Overlaid are a few regions typically considered: plasmonic resonators, antennas, and micropillar cavities (MPCs). The top axis displays the bandwidth of a photonic structure with a given quality factor compared with the line width of typical room-temperature and cryogenic quantum emitters. (CQDs: colloidal quantum dots, SAQDs: self-assembled quantum dots, NV: nitrogen vacancy centers in diamond, SiV: silicon vacancy centers in diamond). (B) Illustration of the nanocone bullseye antenna considered in this study that combines an antenna and resonator for rate and directionality enhancement. FDTD simulations displaying (C) Purcell factor and collection efficiency (NA = 0.5) of a full device with a randomly oriented dipole source over a broad spectral range and (D) the near field intensity of a vertically polarized dipole source displaying a strong enhancement near the nanocone apex resulting in the Purcell enhancement.

and large mode volume are required in order to achieve both directionality and rate enhancement. Nanostructures like these include some mature technologies such as micropillar cavities (MPCs)¹ and photonic crystal cavities.¹⁵ The caveat here, however, is that the high Q factor leads to a restrictively narrow bandwidth, and to match this, the emitter must have an even narrower line width, which is a requirement that is only typically met for emitters operating at cryogenic temperatures such as SAQDs. Even in this case, however, the high Q resonator and low temperature emitter must be tuned into resonance in a postfabrication step, thus limiting the scalability of such approaches. Conversely, at higher temperatures, an efficient structure should have a low Q factor limited by the line width of the emitter. Room-temperature operation therefore limits one to a choice between either antennas (low Q, large V),^{16–19} which provide control over the angular emission pattern, or nanoresonators (low Q, small V)^{20–22} that lead to lifetime reduction. This limitation can be detrimental for the practical implementation of sources based on room-temperature emitters in general.

A few years ago, we suggested a solution to this trade-off by proposing a composite structure shown in Figure 1B that combines a nanocone (used as a plasmonic resonator) and a circular Bragg grating (used as an antenna).²³ In this

composite structure, the emission from an emitter would first couple to the plasmonic nanocone before coupling to the hybrid metal–dielectric bullseye antenna which redirects the emission out-of-plane.²³ These two components were chosen since nanocones have consistently shown the ability to induce large Purcell factors on the order of 100 due to the significant field enhancement near the apex^{24–26} (Figure 1D) and circular Bragg gratings have shown extraordinary results in terms of emission redirection.^{16–19,23,27,28} The combination of the two should therefore be able to perform both required functionalities over a broadband range in a single integrated, compact device as displayed in Figure 1C. This was confirmed in detailed FDTD simulations^{23,29} which showed the promise of such a structure in inducing both a large Purcell factor and large directionality enhancement. In this paper, we realize this composite structure shown in Figure 1B and experimentally overcome the rate-directionality trade-off for single broadband quantum emitters and demonstrate a Purcell factor of 20 alongside record-high directionality, thus demonstrating an ultrafast source of single photons which also has a very high collection efficiency even to low numerical apertures.

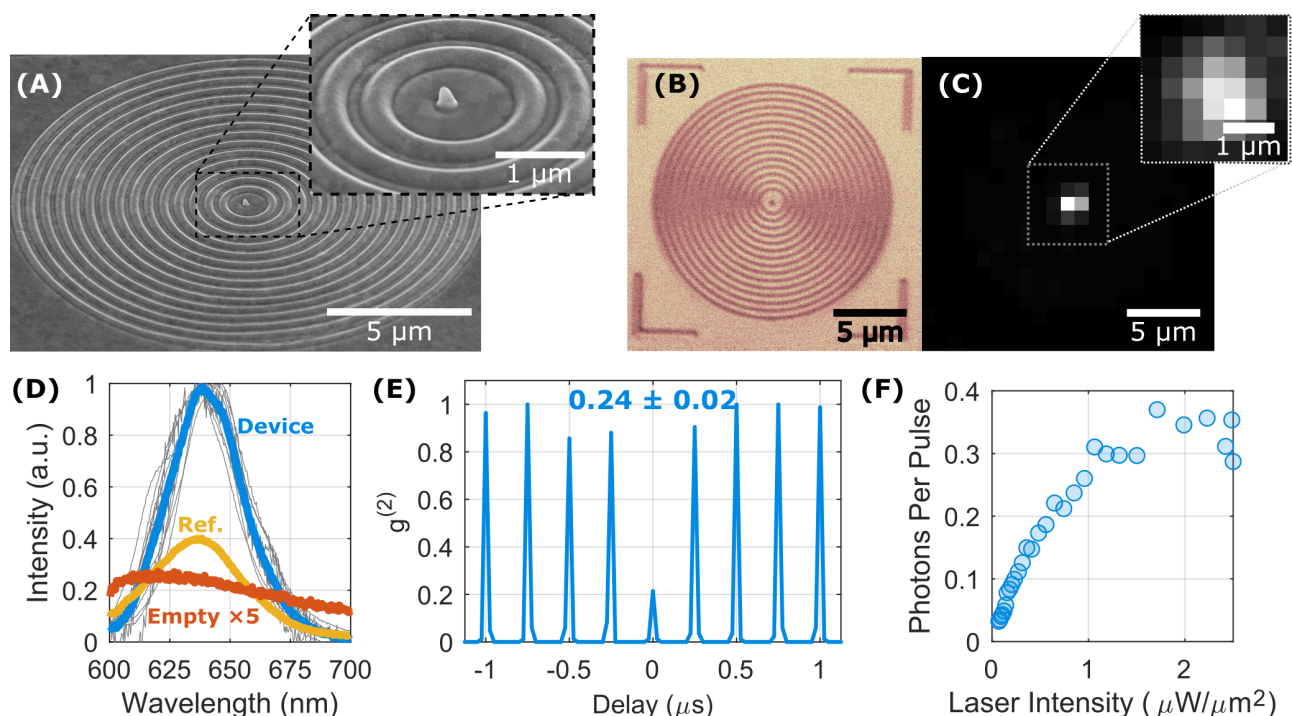


Figure 2. Optical and spectral properties of our operating devices. (A) Scanning electron microscope and (B) optical microscope image of a fabricated device. (C) Confocal scanning fluorescence image displaying emission only from CQDs coupled to the nanocone. (D) Spectrum of 15 different nanocone bullseye antennas containing CQDs (gray) with the average spectrum in blue compared to reference CQDs on glass in yellow and an empty antenna with no CQDs in orange. (E) Time-filtered second order correlation measurement using a Hanbury–Brown–Twiss experiment displaying a single CQD coupled to the device while exciting near saturation (time gate of 2 ns). (F) Single CQD power saturation measurement showing a saturation rate of 0.35 photons/pulse.

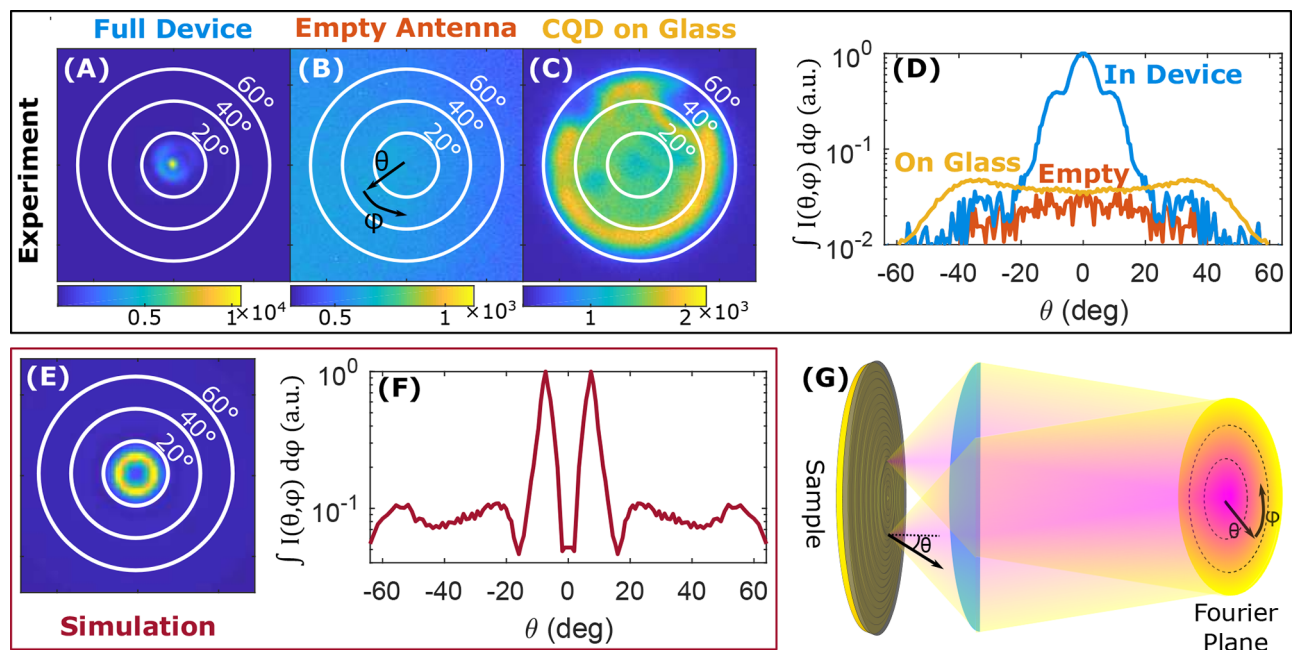


Figure 3. Angular properties of our operating devices. A back focal plane image of (A) a measured fully fabricated device which displays the strong directionality enhancement; (B) an empty antenna; (C) a measured CQD on glass; and (E) a fully simulated device. (D) Experimental and (F) simulated angular intensity profile after integrating for the azimuthal angle ϕ . In (D), all of the curves are normalized to the maximum for the device. (G) Schematic representation of the back focal plane imaging technique used to measure directionality in this study.

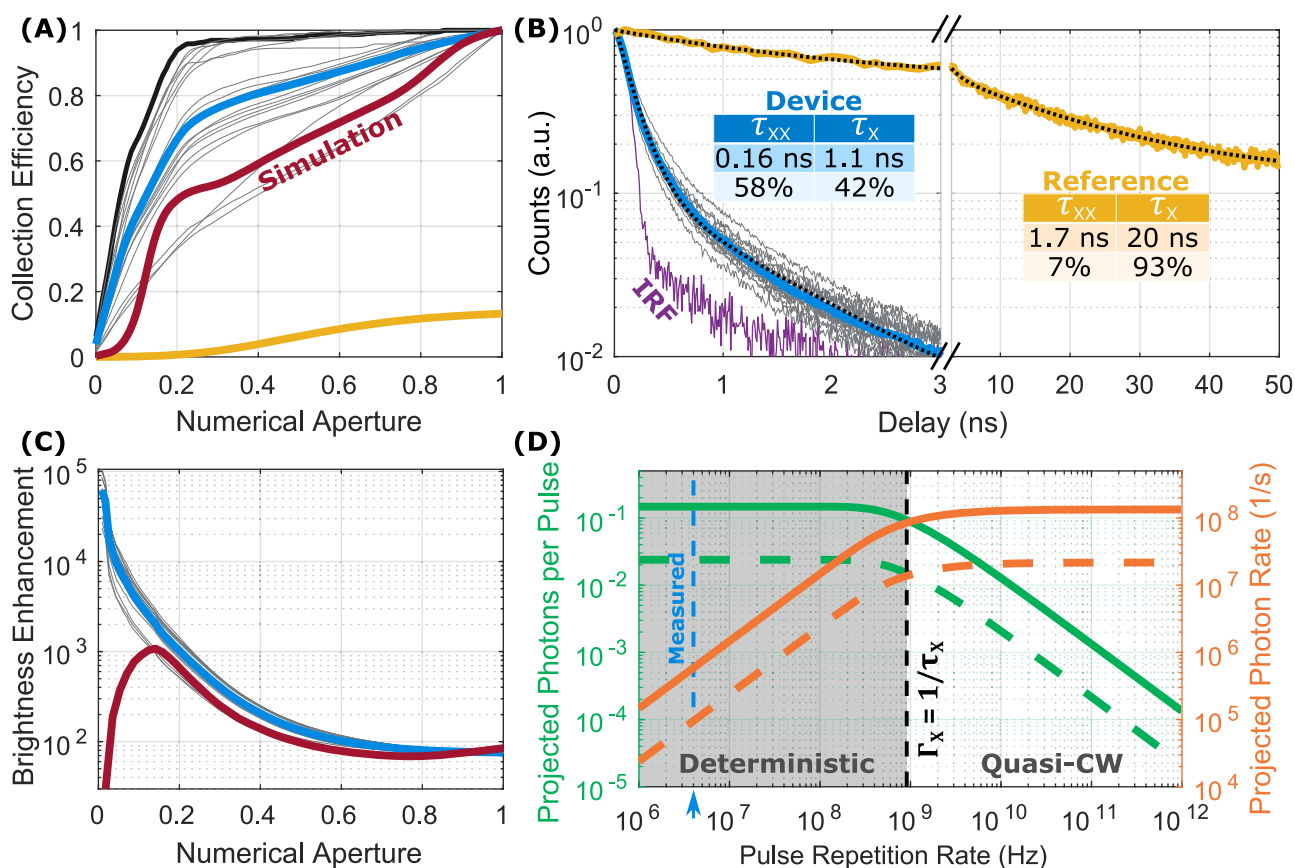


Figure 4. Decay rate and collection efficiency enhancement in our devices. (A) Collection efficiency, (B) lifetime, and (C) brightness enhancement factor measurements for 20 fabricated devices (gray lines) with the average represented in blue and best performing device in black. Yellow lines represent measurements of the same CQDs on glass. The dotted black lines in (D) are biexponential fits for the lifetimes. The purple line represents the instrument response function (IRF) of our system. The red lines represent FDTD simulations of the structure. (D) Projected photons per pulse (green) and projected photon rate (orange) at different excitation laser repetition rates. The solid lines represent single photons originating solely from exciton emission whereas the dashed lines represent the single photon rate after time-gated filtering (2 ns). The blue dashed line represents the repetition rate at which the measurement was made.

RESULTS AND DISCUSSION

The proposed device, shown in Figure 2A, is a combination of an Au plasmonic nanocone located at the center of a hybrid metal-dielectric bullseye antenna. As opposed to our theoretical study²³ the sharpness of the nanocone tip was limited to a diameter of 40 nm due to fabrication constraints (see below). Given the small mode-volume of the nanocone plasmonic resonator, placement with high spatial accuracy is essential in the operation of the device. In our method, the CQDs are bound selectively to the tips of the nanocones using a modified approach based on our previous works (see the Methods and Figure S1).²⁵ This approach ensures that CQDs can be bound to the tip of the nanocone only. A demonstration of this is illustrated in Figure 2B,C, which displays a confocal map showing that fluorescence comes solely from the nanocone region at the center of the bullseye structure. Moreover, this fluorescence is significantly stronger than any plasmonic noise resulting from the underlying structure as shown in Figure 2D. This, in addition to the device spectrum shown, confirms that this is indeed CQD fluorescence.

Single photon emission can only be achieved by successfully binding single CQDs to the tips of the nanocones. In a single CQD, the main contributor to multiphoton emission comes from the biexciton state (XX), which may be filtered temporally using the time-gated filtering technique leading to

nearly ideal single photon emission.^{16,30,31} An example of a device containing a single CQD is shown in Figure 2E, indicating our success in reaching single CQD binding levels. Furthermore, by using the devices in which the number of CQDs are known and conducting power saturation measurements as shown in Figure 2F, we consistently demonstrate a high single photon saturation rate approaching 0.35 photons per CQD per pulse, which indicates high overall efficiency of the device (see Supporting Information).

Figure 3A is a measurement of a back-focal plane image displaying the angular emission pattern from one of the devices. A high directivity of the emission is clearly seen, associated with the coupling of the enhanced CQD emission to the hybrid metal-dielectric bullseye structure. This is contrasted against the results for a structure without any CQDs attached and to CQDs on glass in Figure 3B,C. In Figure 3E,F, this is also compared to an FDTD simulation of the emission of a full device with a randomly oriented dipole positioned 7 nm above the nanocone. The simulation results in a strong enhancement of the *z*-dipole emission and therefore the dominance of the ring-shaped angular emission pattern. Our measured devices, on the other hand, show also significant in-plane dipole emission (see Figure 3D) which can be explained by the lateral displacement of the CQDs on the nanocone. Due to fabrication constraints, the CQDs do not

Table 1. Decay Rates and Enhancement Factors for CQDs

i	Γ_{0i}	Γ_i	F_i	F_i^r	F_i^{nr}	QY_{0i}	QY_i
X	$(20 \pm 1 \text{ ns})^{-1}$	$(1.08 \pm 0.06 \text{ ns})^{-1}$	19 ± 2	9 ± 5	21 ± 7	0.28 ± 0.09	0.147 ± 0.009
XX	$(1.7 \pm 0.1 \text{ ns})^{-1}$	$(0.159 \pm 0.002 \text{ ns})^{-1}$	11 ± 1	23 ± 10	9 ± 1	0.023 ± 0.009	0.203 ± 0.012

necessarily bind exactly to the cone apex, but can be shifted laterally by several nanometers. This asymmetry leads both to a reduction of the Purcell factor for the z -dipole and to an increasing contribution of the x -dipole component, which is radiated upward. This is confirmed by detailed simulations shown in Figure S3. This additional emission near 0° has the effect of further improving the efficiency of the device for photon collection.

This high directionality leads to a significant improvement in the collection efficiency (η_{coll}) from over 20 measured devices as shown in Figure 4A with an average collection efficiency of 84% at NA = 0.5. This is more than 10-fold better than a CQD on glass. This performance improvement is further amplified at even lower NAs where, for example, the collection efficiency at NA = 0.22 (70%) is 88-fold greater than that of the reference (0.8%). Several devices (seven) in Figure 4A also show superior performance compared to the rest with the best device showing a collection efficiency of >95% at an NA of 0.5. These results are in line with our recent report on the high collection efficiencies achievable from CQDs and NV centers positioned in our bare metal–dielectric bullseye antennas without a plasmonic resonator.¹⁶

Unlike our previous works where the CQDs were embedded in an antenna-only structure, and therefore only high directivity was demonstrated, here in Figure 4B we show that this is accompanied by a significant rate enhancement in our devices as compared to a similar CQD on glass. The long lifetime component (associated with the exciton (X) state of the CQD) was reduced from 20 to 1.1 ns, whereas the shorter lifetime component (biexciton (XX) state) was reduced from 1.7 to 0.16 ns. The reduction in lifetime also brings about a significant change in the quantum efficiency of different states in the QD. In a reference CQD only about 7% of the emission results from the XX state due to nonradiative Auger recombination processes which successfully compete with the XX radiative channel. On the other hand, the XX state accounts for 58% of the emission in our composite device which is mainly attributed to the shortening of the radiative lifetime of the XX state to a degree that is comparable to the Auger recombination rate. This is a well-known phenomenon that has been previously reported in several studies^{26,32–34} and will be confirmed below.

To quantitatively extract the radiative rate enhancement, and to explain the change in the XX state contribution in lifetime curves, we analyzed the set of rate equations associated with the device (cf. the Supporting Information). A modification of the photonic environment near an emitter can lead to a change in the radiative (Γ_i^r) and nonradiative (Γ_i^{nr}) decay rates of the i th state in the emitter ($i = X, XX$) leading to an overall decay rate $\Gamma_i = \Gamma_i^r + \Gamma_i^{nr}$. This modification compared to the rate in free space Γ_{0i} (known as the Purcell factor F_i), is attributed to radiative (F_i^r) and nonradiative (F_i^{nr}) enhancement factors given by^{23,26}

$$\Gamma_i = F_i \Gamma_{0i} = \underbrace{F_i^r \Gamma_{0i}^r}_{\Gamma_i^r} + \underbrace{F_i^{nr} \Gamma_{0i}^{nr} + \Gamma_{0i}^{nr}}_{\Gamma_i^{nr}} \quad (1)$$

The intrinsic quantum yield $QY_{0i} = \Gamma_{0i}^r / \Gamma_{0i}$ of the CQD is therefore altered to result in a device quantum yield $QY_i = \Gamma_i^r / \Gamma_i$. By fitting the time-resolved measurements to a biexponential decay curve (derived from the rate equations) and using the overall quantum yield of the device (obtained from power saturation measurements), we extract both the radiative and nonradiative enhancement factors for the X and XX state in our device as summarized in Table 1. The extracted overall Purcell factors (F) of the order of 20 are a further confirmation of the capability of our devices to increase the decay rate of the emitters. Critically, this enhancement is mainly due to an increase in radiative channels with measured radiative enhancement factors (F^r) between 10 and 20. This results in device quantum yields (Table 1) that are either slightly lower (X state) or significantly higher (XX state) than in the reference CQD and explains the relatively high photon fluxes measured above (0.35 photons/pulse). A detailed FDTD simulation of the current device, however, predicts that the Purcell factor for a vertically oriented dipole emitter should be >40 while a horizontally oriented dipole exhibits no enhancement. This discrepancy is likely due to imperfections in the nanocone and probably contributes to the difference in the expected angular emission pattern, where the dominance in vertically polarized as opposed to in-plane polarized emission is not seen experimentally (see a detailed discussion about this in the Supporting Information).

The dual role of our device, *i.e.*, both high Purcell factor and high collection efficiency, leads to a significant enhancement in the usable photon rate that can be collected from the device by an optical system with a given numerical aperture. To quantify this improvement, we introduce a brightness enhancement factor for the single excitonic photon emission rate shown in Figure 4C (see the Supporting Information):

$$\text{BE(NA)} = \frac{QY_X \Gamma_X \eta_{\text{coll}}(\text{NA}) \leftarrow \text{rate in device}}{QY_{0X} \Gamma_{0X} \eta_{0,\text{coll}}(\text{NA}) \leftarrow \text{rate on glass}} \quad (2)$$

Figure 4C shows the brightness enhancement factor measurements for 20 fabricated devices. Clearly, the structure results in a significant increase of single photon fluxes reaching factors of 10^3 – 10^5 at low NA (<0.2), 130 at NA = 0.5, and 80 at NA = 1. At the laser repetition rate we used in our experiment (4 MHz) we measured a single photon rate of 0.6 MHz into our objective lens (NA = 0.9) resulting from the X state. Since the actual rate of collected photons in our experiment was limited only by the rate of the pump laser (4 MHz), we show in Figure 4D the projected single photon rate *vs* the laser repetition rate by extrapolating the results we obtained at a repetition rate of 4 MHz and calculating the expected photon rates resulting from the exciton emission only (see the Supporting Information). The solid lines represent the projected photon rates from the exciton emission *only* but without any filtering of the biexciton photons and other short lifetime noise photons. While this yields an upper bound of exciton emission rates, the single photon purity of such a device will be limited by multiphoton emission.³¹ We therefore plot in the dashed line the projected exciton emission rate with

passive time gated filtering,^{30,35} which as shown in Figure 2E, rejects most of the biexciton and other noise photons. This results in a reduced photon rate by a factor of 0.16. We note that while this still yields rates as high as 2×10^7 photons/second, it is only a lower bound for the achievable high purity single photon rates. This is because the passive time-gated filtering technique is rather inefficient due to the relatively high biexciton quantum yield. Recently, we have suggested heralded purification methods to resolve this inefficiency.³¹ These methods are particularly tailored to purifying the emission when both exciton and biexciton quantum yields are high as is expected when the Purcell factor is increased due to more optimized devices. Therefore, these techniques are expected to play a major role in such enhanced devices. Other ways to increase the purity are by using spectral filtering of the X line in type-II CQDs which exhibit a large X–XX splitting,^{36,37} or in cryogenic CQDs.

As can be seen from Figure 4E, in the regime where the laser repetition rate is smaller than the X decay rate (Γ_X), the time between pulses is sufficient to allow the CQD to relax completely and therefore the emission is more deterministic with rates expected to approach 1.0×10^8 photons/second. On the other hand, in the quasi-CW regime, where the laser repetition rate is higher than Γ_X , the achievable photon rates approach 1.4×10^8 photons/s. Therefore, such devices should enable high photon rates from single quantum emitters at room temperature approaching the GHz regime.

These results can be improved by further optimizing our devices. First, commercial CQDs were used with time stable operation of several minutes (Figure S2C). This can be further extended by replacing these CQDs with giant core/shell CQDs¹³ as demonstrated in our recent publication¹⁶ where giant CQDs were placed in similar bullseye devices without nanocones, resulting in record high collection efficiency of single photons together with reduced blinking and very stable operation over hours of continuous excitation without any observed optical degradation. The blinking observed in this work thus presents no general limitation for the shown hybrid devices. Furthermore, the tip radius in our case, was limited by the spot diameter (~ 40 nm) of our Focused Ion Beam (FIB) machine used to produce the template. This broad tip size results in a smaller Purcell factor due to the smaller field enhancement near the tip. Previously, sharper tipped cones were produced using electron beam methods.^{24,25} The template stripping method used here, on the other hand, enables the production of many higher quality samples from a single template containing both the nanocone and bullseye.^{16,38} Still, much sharper nanocones can be fabricated (down to 7.5 nm²⁶) by employing commercial FIB machines with much smaller beam sizes which would improve the predicted photon enhancement even further²³ as well as increase the yield of single CQD binding.

We note that existing solutions based on pure plasmonic antennas and resonators^{39,40} have a significant trade-off between directionality and device optical yield. This is due to the large propagation losses of the surface plasmon polaritons. For high directionality, a large antenna area is required. Due to the high propagation losses of surface plasmons at the visible and near-IR, this unavoidably leads to a reduction in the optical quantum yield of the device. In contrast, here we achieve both rate and directionality enhancement in room-temperature emitters while showing experimentally that the plasmonic enhancer has not signif-

cantly altered the emitter's quantum efficiency. This is the advantage of the hybrid solution, where the rate enhancement is plasmonic-based, but the large antenna is low-loss dielectric-based.

CONCLUSIONS

To summarize, we have demonstrated effective decay rate and directionality enhancement on few and single room-temperature emitters. This is a significant step in solving the many obstacles facing the practical use of room-temperature sources. The projected photon rates that have been reported here are realistically approaching the GHz emission range that is needed for future quantum applications.¹⁰ Two main fields that may benefit from such incoherent photon guns are quantum metrology and cryptography. Using these highly intensity-squeezed sources, weak absorption measurements on highly sensitive samples or for calibrating photodetectors with high precision well beyond the shot-noise limit may be performed, setting the standard for intensity measurements known as the quantum candela.⁴¹ In quantum key distribution, single photon sources with rates that can approach the GHz regime are essential as the ultimate solution for robust high rate transmission resistant against the photon number splitter attack as well as other active attacks on weak coherent sources. The compact and scalable on-chip concept demonstrated here can be easily implemented on other photon sources. The very broadband nature of our composite device relaxes the stringent challenge of matching the resonant frequency of high-Q resonators to the emission frequencies of the emitters, which typically vary from emitter to emitter randomly. This will allow scaling up many emitters on one predesigned chip with a high yield. We expect that such scaling will help in developing quantum light–matter interfaces.

METHODS

The metallic part of the device was fabricated in a similar manner to what was reported in ref 16 using the template stripping method.³⁸ A silicon substrate was cleaned using Piranha and acetone to be used as the template. An inverted nanocone was etched into the silicon substrate using a 1.1 pA Ga ion beam. Around this nanocone the bullseye was etched using a 240 pA Ga ion beam. Gold (250 nm) was then deposited on the template, followed by spin coating of SU8 3010 at 3000 rpm which was prebaked at 95 °C for 5 min. A glass slide was then attached, and the SU8 was cured with UV at 150 mJ/cm² for 15 s flood exposure. The Au attached to the glass was stripped off the template due to the low adhesion between silicon and Au, resulting in very smooth bullseye antennas.

The resulting nanocone is higher than the rings (180 nm vs 100 nm) as shown in Figure S1. This enables the attachment of quantum dots (CdSe/ZnS core/shell type, diameter 8 nm, emission wavelength 650 nm, purchased from PlasmaChem GmbH) following a modified protocol previously described in refs 24 and 25. The sample was embedded in poly(methyl methacrylate) (PMMA) in a two-step spin coating process with an intermediate and final prebaking step (5 min, 90 °C). The obtained height of 220 nm is sufficient to fully cover the nanocones. Subsequently, the PMMA was etched using a directed oxygen–plasma (reactive ion etching (RIE), Plasmalab 80 Plus, Oxford Instruments, 45 s, 20 W, 0.1 Torr) to uncover only the tips of the cones. The sample was then placed in 3-mercaptopropionic acid (3-MPA, purchased from SigmaAldrich, 10 mM, 30 min) diluted in water to adsorb a self-assembled monolayer on the gold tips acting as linker molecules. Afterward it was exposed to a QD solution in hexane (10 μ g ml⁻¹, 24 h). The CQDs' ligand shell consisting of trioctylphosphine oxide (TOPO) and hexadecylamine (HDA) binds to the 3-MPA. Excess CQDs and PMMA were removed by rinsing in

acetone and isopropyl alcohol. Finally, a capping layer of 570 nm of PMMA was added to constitute the waveguide layer.

The setup used in the experiment is discussed in detail in the Supporting Information of ref 16. A 4 MHz pulsed 405 nm laser was used for excitation for the majority of the experiments. There are several reasons why pulsed operation was chosen. First, pulsed operation offers the unique benefit of on-demand generation of photons which is a very important property of any future quantum device as has been demonstrated in applications of boson sampling,³ quantum computation,^{4–7} and quantum key distribution.⁸ On the other hand, CW excitation creates a randomly arriving stream of photons which is of less use. Second, the pulsed nature of the excitation enables temporal separation between the short-lifetime components (noise and multiexciton emission) and the relevant signal (exciton emission), without significant loss of single photon brightness. The saturation curves were obtained by scanning the average power of this pulsed laser and monitoring the resulting photon rates measured at the single photon detectors. This photon rate is normalized by the system efficiency (~20%) to yield the photon rate into the NA of our objective. In the devices in which the number of CQDs was known (from a second order correlation measurement, see the Supporting Information), this saturation curve was also normalized by the number of CQDs to yield photons/pulse/CQD.

The number of CQDs in a device is determined using a time-gated filtering technique^{30,31,35} (time-gate of 2 ns) which differentiates between multiexciton and multiple-CQD emission in a second-order correlation measurement. Single and few CQD devices were used to determine the overall quantum yield (see the Supporting Information). The remaining measurements (lifetime, X–XX composition, Purcell factors, and directionality) were done on these devices in addition to multiple-CQD devices.

ASSOCIATED CONTENT

Supporting Information

The Supporting Information is available free of charge at <https://pubs.acs.org/doi/10.1021/acsnano.1c08591>.

Details regarding the CQD number statistics, the lateral CQD displacement, the enhancement rate calculation, and the photon rate extrapolation in addition to supporting figures displaying the binding method, the photostability of the CQDs, and the decay rate dependence on lateral displacement (PDF)

AUTHOR INFORMATION

Corresponding Author

Ronen Rapaport – *Racah Institute of Physics, The Hebrew University of Jerusalem, Jerusalem 9190401, Israel; The Center for Nanoscience and Nanotechnology and The Applied Physics Department, The Hebrew University of Jerusalem, Jerusalem 9190401, Israel; Email: ronnr@phys.huji.ac.il*

Authors

Hamza Abudayyeh – *Racah Institute of Physics, The Hebrew University of Jerusalem, Jerusalem 9190401, Israel; The Center for Nanoscience and Nanotechnology, The Hebrew University of Jerusalem, Jerusalem 9190401, Israel; orcid.org/0000-0003-2164-6700*

Annika Mildner – *Institute for Applied Physics and Center LISA⁺, University of Tuebingen, 72076 Tuebingen, Germany*

Dror Liran – *Racah Institute of Physics, The Hebrew University of Jerusalem, Jerusalem 9190401, Israel; The Center for Nanoscience and Nanotechnology, The Hebrew University of Jerusalem, Jerusalem 9190401, Israel; orcid.org/0000-0002-4452-5058*

Boaz Lubotzky – *Racah Institute of Physics, The Hebrew University of Jerusalem, Jerusalem 9190401, Israel; The Center for Nanoscience and Nanotechnology, The Hebrew University of Jerusalem, Jerusalem 9190401, Israel*
Lars Lüder – *Institute for Applied Physics and Center LISA⁺, University of Tuebingen, 72076 Tuebingen, Germany; Present Address: Swiss Federal Laboratories for Materials Science and Technology, 9014 St. Gallen, Switzerland*
Monika Fleischer – *Institute for Applied Physics and Center LISA⁺, University of Tuebingen, 72076 Tuebingen, Germany*

Complete contact information is available at: <https://pubs.acs.org/10.1021/acsnano.1c08591>

Notes

The authors declare no competing financial interest.

ACKNOWLEDGMENTS

Financial support by COST (European Cooperation in Science and Technology) Action MP1302 and the Germany Excellence Initiative is gratefully acknowledged. R.R. acknowledges support from the Israeli Innovation Authority: Quantum Communication Consortium. The authors thank the Center for Nanoscience and Nanotechnology at the Hebrew University of Jerusalem for their support in fabricating and characterizing the samples in this paper.

REFERENCES

- (1) Somaschi, N.; Giesz, V.; De Santis, L.; Loredo, J. C.; Almeida, M. P.; Hornecker, G.; Portalupi, S. L.; Grange, T.; Anton, C.; Demory, J.; Gomez, C.; Sagnes, I.; Kimura, N. D. L.; Lemaitre, A.; Auffeves, A.; White, A. G.; Lanco, L.; Senellart, P. Near Optimal Single Photon Sources in the Solid State. *Nat. Photonics* **2016**, *10*, 340–345.
- (2) Meyer-Scott, E.; Silberhorn, C.; Migdall, A. Single-Photon Sources: Approaching the Ideal Through Multiplexing. *Rev. Sci. Instrum.* **2020**, *91*, 041101.
- (3) Wang, H.; Qin, J.; Ding, X.; Chen, M.-C.; Chen, S.; You, X.; He, Y.-M.; Jiang, X.; You, L.; Wang, Z.; Schneider, C.; Renema, J. J.; Höfling, S.; Lu, C.-Y.; Pan, J.-W. Boson Sampling With 20 Input Photons and a 60-Mode Interferometer in a 10^{14} -Dimensional Hilbert Space. *Phys. Rev. Lett.* **2019**, *123*, 250503.
- (4) Pooley, M. A.; Ellis, D. J.; Patel, R. B.; Bennett, A. J.; Chan, K. H.; Farrer, I.; Ritchie, D. A.; Shields, A. J. Controlled-Not Gate Operating With Single Photons. *Appl. Phys. Lett.* **2012**, *100*, 211103.
- (5) He, Y.-M.; He, Y.; Wei, Y.-j.; Wu, D.; Atatüre, M.; Schneider, C.; Höfling, S.; Kamp, M.; Lu, C.-y.; Pan, J.-w. On-Demand Semiconductor Single-Photon Source With Near-Unity Indistinguishability. *Nat. Nanotechnol.* **2013**, *8*, 213–217.
- (6) Schwartz, I.; Cogan, D.; Schmidgall, E. R.; Don, Y.; Gantz, L.; Kenneth, O.; Lindner, N. H.; Gershoni, D. Deterministic Generation of a Cluster State of Entangled Photons. *Science* **2016**, *354*, 434–437.
- (7) Istrati, D.; Pilnyak, Y.; Loredo, J. C.; Antón, C.; Somaschi, N.; Hilaire, P.; Ollivier, H.; Esmann, M.; Cohen, L.; Vidro, L.; Millet, C.; Lemaitre, A.; Sagnes, I.; Harouri, A.; Lanco, L.; Senellart, P.; Eisenberg, H. S. Sequential Generation of Linear Cluster States From a Single Photon Emitter. *Nat. Commun.* **2020**, DOI: [10.1038/s41467-020-19341-4](https://doi.org/10.1038/s41467-020-19341-4).
- (8) Takemoto, K.; Nambu, Y.; Miyazawa, T.; Sakuma, Y.; Yamamoto, T.; Yorozu, S.; Arakawa, Y. Quantum Key Distribution Over 120 Km Using Ultrahigh Purity Single-Photon Source and Superconducting Single-Photon Detectors. *Sci. Rep.* **2015**, *5*, 14383.
- (9) Yin, J.; Cao, Y.; Li, Y.-H.; Liao, S.-K.; Zhang, L.; Ren, J.-G.; Cai, W.-Q.; Liu, W.-Y.; Li, B.; Dai, H.; Li, G.-B.; Lu, Q.-M.; Gong, Y.-H.; Xu, Y.; Li, S.-L.; Li, F.-Z.; Yin, Y.-Y.; Jiang, Z.-Q.; Li, M.; Jia, J.-J.; et al. Satellite-Based Entanglement Distribution Over 1200 Kilometers. *Science* **2017**, *356*, 1140–1144.

- (10) Aharonovich, I.; Englund, D.; Toth, M. Solid-State Single-Photon Emitters. *Nat. Photonics* **2016**, *10*, 631–641.
- (11) Michler, P.; Kiraz, A.; Becher, C.; Schoenfeld, W. V.; Petroff, P. M.; Zhang, L.; Hu, E.; Imamoglu, A. A Quantum Dot Single-Photon Turnstile Device. *Science* **2000**, *290*, 2282–2285.
- (12) Aharonovich, I.; Neu, E. Diamond Nanophotonics. *Adv. Opt. Mater.* **2014**, *2*, 911–928.
- (13) Chen, Y.; Vela, J.; Htoon, H.; Casson, J. L.; Werder, D. J.; Bussiss, D. A.; Klimov, V. I.; Hollingsworth, J. A. "Giant" Multishell CdSe Nanocrystal Quantum Dots With Suppressed Blinking. *J. Am. Chem. Soc.* **2008**, *130*, 5026–5027.
- (14) Panfil, Y. E.; Oded, M.; Banin, U. Colloidal Quantum Nanostructures: Emerging Materials for Display Applications. *Angew. Chem., Int. Ed.* **2018**, *57*, 4274–4295.
- (15) Liu, F.; Brash, A. J.; O'Hara, J.; Martins, L. M. P. P.; Phillips, C. L.; Coles, R. J.; Royall, B.; Clarke, E.; Bentham, C.; Prtljaga, N.; Itskevich, I. E.; Wilson, L. R.; Skolnick, M. S.; Fox, A. M. High Purcell Factor Generation of Indistinguishable on-Chip Single Photons. *Nat. Nanotechnol.* **2018**, *13*, 835–840.
- (16) Abudayyeh, H.; Lubotzky, B.; Blake, A.; Wang, J.; Majumder, S.; Hu, Z.; Kim, Y.; Htoon, H.; Bose, R.; Malko, A. V.; Hollingsworth, J. A.; Rapaport, R. Single Photon Sources With Near Unity Collection Efficiencies by Deterministic Placement of Quantum Dots in Nanoantennas. *APL Photonics* **2021**, *6*, 036109.
- (17) Rickert, L.; Kupko, T.; Rodt, S.; Reitzenstein, S.; Heindel, T. Optimized Designs for Telecom-Wavelength Quantum Light Sources Based on Hybrid Circular Bragg Gratings. *Opt. Express* **2019**, *27*, 36824.
- (18) Liu, J.; Su, R.; Wei, Y.; Yao, B.; Silva, S. F. C. d.; Yu, Y.; Iles-Smith, J.; Srinivasan, K.; Rastelli, A.; Li, J.; Wang, X. A Solid-State Source of Strongly Entangled Photon Pairs With High Brightness and Indistinguishability. *Nat. Nanotechnol.* **2019**, *14*, 586–593.
- (19) Wang, H.; Hu, H.; Chung, T.-H.; Qin, J.; Yang, X.; Li, J.-P.; Liu, R.-Z.; Zhong, H.-S.; He, Y.-M.; Ding, X.; Deng, Y.-H.; Dai, Q.; Huo, Y.-H.; Höfling, S.; Lu, C.-Y.; Pan, J.-W. On-Demand Semiconductor Source of Entangled Photons Which Simultaneously Has High Fidelity, Efficiency, and Indistinguishability. *Phys. Rev. Lett.* **2019**, *122*, 113602.
- (20) Ji, B.; Giovanelli, E.; Habert, B.; Spinicelli, P.; Nasilowski, M.; Xu, X.; Lequeux, N.; Hugonin, J.-P.; Marquier, F.; Greffet, J.-J.; Dubertret, B. Non-Blinking Quantum Dot With a Plasmonic Nanoshell Resonator. *Nat. Nanotechnol.* **2015**, *10*, 170–175.
- (21) Hoang, T. B.; Akselrod, G. M.; Mikkelsen, M. H. Ultrafast Room-Temperature Single Photon Emission From Quantum Dots Coupled to Plasmonic Nanocavities. *Nano Lett.* **2016**, *16*, 270–275.
- (22) Dhawan, A. R.; Belacel, C.; Esparza-Villa, J. U.; Nasilowski, M.; Wang, Z.; Schwob, C.; Hugonin, J.-P.; Coolen, L.; Dubertret, B.; Senellart, P.; Maitre, A. Extreme Multiexciton Emission From Deterministically Assembled Single-Emitter Subwavelength Plasmonic Patch Antennas. *Light: Sci. Appl.* **2020**, *9*, 33.
- (23) Abudayyeh, H.; Rapaport, R. Quantum Emitters Coupled to Circular Nanoantennas for High Brightness Quantum Light Sources. *Quantum Science and Technology* **2017**, *2*, 034004.
- (24) Fulmes, J.; Jäger, R.; Bräuer, A.; Schäfer, C.; Jäger, S.; Gollmer, D. A.; Horrer, A.; Nadler, E.; Chassé, T.; Zhang, D.; Meixner, A. J.; Kern, D. P.; Fleischer, M. Self-Aligned Placement and Detection of Quantum Dots on the Tips of Individual Conical Plasmonic Nanostructures. *Nanoscale* **2015**, *7*, 14691–14696.
- (25) Meixner, A. J.; Jäger, R.; Jäger, S.; Bräuer, A.; Scherzinger, K.; Fulmes, J.; Krockhaus, S. z. O.; Gollmer, D. A.; Kern, D. P.; Fleischer, M. Coupling Single Quantum Dots to Plasmonic Nanocones: Optical Properties. *Faraday Discuss.* **2015**, *184*, 321–337.
- (26) Matsuzaki, K.; Vassant, S.; Liu, H.-W.; Dutschke, A.; Hoffmann, B.; Chen, X.; Christiansen, S.; Buck, M. R.; Hollingsworth, J. A.; Göttinger, S.; Sandoghdar, V. Strong Plasmonic Enhancement of Biexciton Emission: Controlled Coupling of a Single Quantum Dot to a Gold Nanocone Antenna. *Sci. Rep.* **2017**, *7*, 42307.
- (27) Livneh, N.; Harats, M. G.; Istrati, D.; Eisenberg, H. S.; Rapaport, R. Highly Directional Room-Temperature Single Photon Device. *Nano Lett.* **2016**, *16*, 2527–2532.
- (28) Harats, M. G.; Livneh, N.; Rapaport, R. Design, Fabrication and Characterization of a Hybrid Metal-Dielectric Nanoantenna With a Single Nanocrystal for Directional Single Photon Emission. *Opt. Mater. Express* **2017**, *7*, 834.
- (29) Lumerical Solutions, Inc. <http://www.lumerical.com/tcad-products/fdtd/>.
- (30) Mangum, B. D.; Ghosh, Y.; Hollingsworth, J. A.; Htoon, H. Disentangling the Effects of Clustering and Multi-Exciton Emission in Second-Order Photon Correlation Experiments. *Opt. Express* **2013**, *21*, 7419–26.
- (31) Abudayyeh, H.; Lubotzky, B.; Majumder, S.; Hollingsworth, J. A.; Rapaport, R. Purification of Single Photons by Temporal Heralding of Quantum Dot Sources. *ACS Photonics* **2019**, *6*, 446–452.
- (32) Park, Y.-S.; Ghosh, Y.; Xu, P.; Mack, N. H.; Wang, H.-L.; Hollingsworth, J. A.; Htoon, H. Single-Nanocrystal Photoluminescence Spectroscopy Studies of Plasmon–Multiexciton Interactions at Low Temperature. *J. Phys. Chem. Lett.* **2013**, *4*, 1465–1470.
- (33) Wang, F.; Karan, N. S.; Nguyen, H. M.; Ghosh, Y.; Sheehan, C. J.; Hollingsworth, J. A.; Htoon, H. Correlated Structural-Optical Study of Single Nanocrystals in a Gap-Bar Antenna: Effects of Plasmonics on Excitonic Recombination Pathways. *Nanoscale* **2015**, *7*, 9387–9393.
- (34) Dey, S.; Zhao, J. Plasmonic Effect on Exciton and Multiexciton Emission of Single Quantum Dots. *J. Phys. Chem. Lett.* **2016**, *7*, 2921–2929.
- (35) Feng, S.-W.; Cheng, C.-Y.; Wei, C.-Y.; Yang, J.-H.; Chen, Y.-R.; Chuang, Y.-W.; Fan, Y.-H.; Chuu, C.-S. Purification of Single Photons From Room-Temperature Quantum Dots. *Phys. Rev. Lett.* **2017**, *119*, 143601.
- (36) Achermann, M.; Hollingsworth, J. A.; Klimov, V. I. Multiexcitons Confined Within a Subexcitonic Volume: Spectroscopic and Dynamical Signatures of Neutral and Charged Biexcitons in Ultrasmall Semiconductor Nanocrystals. *Phys. Rev. B: Condens. Matter Mater. Phys.* **2003**, *68*, 245302.
- (37) Ivanov, S. A.; Achermann, M. Spectral and Dynamic Properties of Excitons and Biexcitons in Type-II Semiconductor Nanocrystals. *ACS Nano* **2010**, *4*, 5994.
- (38) Nagpal, P.; Lindquist, N. C.; Oh, S.-H.; Norris, D. J. Ultrasmooth Patterned Metals for Plasmonics and Metamaterials. *Science* **2009**, *325*, 594–7.
- (39) Harats, M. G.; Livneh, N.; Zaiats, G.; Yochelis, S.; Paltiel, Y.; Lifshitz, E.; Rapaport, R. Full Spectral and Angular Characterization of Highly Directional Emission From Nanocrystal Quantum Dots Positioned on Circular Plasmonic Lenses. *Nano Lett.* **2014**, *14*, 5766–5771.
- (40) Yang, G.; Shen, Q.; Niu, Y.; Wei, H.; Bai, B.; Mikkelsen, M. H.; Sun, H. Unidirectional, Ultrafast, and Bright Spontaneous Emission Source Enabled by a Hybrid Plasmonic Nanoantenna. *Laser Photonics Rev.* **2020**, *14*, 1900213.
- (41) Cheung, J. Y.; Chunnillal, C. J.; Woolliams, E. R.; Fox, N. P.; Mountford, J. R.; Wang, J.; Thomas, P. J. The Quantum Candela: A Re-Definition of the Standard Units for Optical Radiation. *J. Mod. Opt.* **2007**, *54*, 373–396.